A double-barrier heterostructure generator of terahertz phonons: many-body effects

2000 J. Phys.: Condens. Matter 12 3149

(http://iopscience.iop.org/0953-8984/12/13/322)

J. Phys.: Condens. Matter **12** (2000) 3149–3172. Printed in the UK PII: S0953-8984(00)03151-9

A double-barrier heterostructure generator of terahertz phonons: many-body effects

Sergio S Makler†‡, I Camps†‖, José Weberszpil‡ and Diana E Tuyarot§

† Instituto de Física, Universidade Federal Fluminense, Campus da Praia Vermelha, Avenida General Milton Tavares de Souza s/n, 24210-340, Niterói, RJ, Brazil
‡ Instituto de Física, Universidade do Estado do Rio de Janeiro, Rua São Francisco Xavier 524, 20550-013 Rio de Janeiro, Brazil
§ Instituto de Física, Universidade Federal do Rio de Janeiro, Cidade Universitária, CT, Bloco A, Caixa Postal 68.528, 21945-970, Ilha do Fundão, RJ, Brazil

E-mail: sergio@if.uff.br

Received 30 March 1999, in final form 11 January 2000

Abstract. In this paper we study the generation of coherent terahertz phonons in a double-barrier heterostructure (DBH) under the influence of an external applied bias. The system is characterized by an energy difference between the two lowest levels in the well, which resonates with the optical phonon energy, producing a high rate of emission of longitudinal optical (LO) phonons. The strong electron–phonon interaction in a polar semiconductor leads to the formation of a polaron that is relevant close to this resonance. Therefore the levels corresponding to the first excited state and the satellite of the ground state anticross in two polaronic branches. The LO phonon has a very short lifetime. It decays by stimulated emission of a pair of phonons (LO $\rightarrow$ $\widetilde{\text{LO}}$ + TA) (where TA stands for transverse acoustic). As a consequence an intense beam of TA coherent phonons is produced, which could have several important applications. A rough model of this system has already been presented (Makler S S, Vasilevskiy M I, Weberszpil J, Anda E V, Tuyarot D E and Pastawski H M 1998 *J. Phys.: Condens. Matter* **10** 5905). Several improvements to that model are presented here. Besides the more accurate treatment of the electron–phonon interaction, the phonon–phonon interaction is considered here taking into account the fact that the whole system is out of equilibrium. The results confirm that the proposed phonon laser is reliable.

1. Introduction

In the last few years the study of double-barrier heterostructures (DBH) has been of great interest from the pure and applied points of view. The relevance of DBH to potential new device applications has been extensively discussed [1].

The pioneering work of Goldman, Tsui and Cunningham [2] has emphasized the great importance that the electron–phonon interaction has as regards the transport properties in mesoscopic double-barrier heterostructures. This is due to the fact that for polar semiconductors, such as GaAs, the dynamical polarization generated by the LO phonon inside the well interacts strongly with the electrons moving along the heterostructure [3, 4].

There have been several theoretical studies on this subject, describing the system by simplified microscopic models solved by using scattering theory [5], the transfer Hamiltonian [6], the Landauer–Büttiker formalism [7] or the direct diagonalization of a tight-binding Hamiltonian [8, 9] to obtain the currents flowing under the influence of an external potential.

‖ Permanent address: Physics Faculty, IMRE, University of Havana, San Lázaro y L, 10400 Havana, Cuba.

0953-8984/00/133149+24$30.00

A treatment of the many-body effects and of the thermodynamical non-equilibrium problem assuming a more realistic model was possible using the Keldysh formalism [10]. Quantum wires and DBH were studied under various conditions such as with applied external magnetic fields, different doping profiles and barrier symmetries, looking for the enhancement of the effects produced by the electron–phonon interaction [11, 12].

These studies were concerned essentially with the way in which the electron–phonon interaction modifies the electronic current. The emission of phonons was a secondary by-product and, as a consequence, little importance was given to the study of their generation, the way in which they propagate and their decay process.

We show here that the generation of phonons can be the central phenomenon taking place in some polar semiconductor DBH under the influence of an external applied potential.

As the electric field is in general large, the system is very far from thermodynamical equilibrium and it is not possible to study the electrons using concepts such as the Fermi level, which are appropriate for describing equilibrium situations. In most cases the phonon population can be considered to be at equilibrium because the electric field does not directly perturb the bosonic degrees of freedom. This has been the approach taken by almost all of the works mentioned previously. However, this assumption is not applicable for a system where almost all electrons suffer inelastic phonon scattering producing a large out-of-equilibrium phonon population spectrum. This is the case, for instance, for an electronic system possessing a characteristic energy that resonates with the energy of the phonon degrees of freedom. A similar situation arises in a resonant tunnelling experiment if the satellite peak is as large as the main resonance current peak due to a significant barrier asymmetry [11]. In these circumstances the phonon populations have to be calculated self-consistently, considering the non-equilibrium situation for both subsystems: electrons and phonons. A rather involved (although rigorous) way of treating this problem is through the application of the Keldysh formalism [10].

The paper is organized as follows. In the next section the DBH phonon laser is described. In section 3 the polaronic model is presented. Section 4 is devoted to showing the method used to solve our Hamiltonian. In section 5 we discuss the kinetic equations for the populations in the system. Finally, in section 6 we present the results and our conclusions.

2. The DBH phonon laser

Recently, we proposed a double-barrier phonon laser [13–15]. It was called a saser, as it is in many respects the phonon analogue of the photon laser beam. The saser could be made, in principle, from a wide variety of materials. We discuss here the particular case of a structure made of GaAs–AlGaAs. This material is simple to grow by molecular beam epitaxy. Besides, in GaAs the decay of LO phonons produces TA phonons [16]. In contrast, in InP the decay of LO phonons produces a pair of LA phonons [17] that will eventually decay because there are other phonon branches of lower energy. On the other hand, TA phonons have a long lifetime and a mean free path greater than 1 mm [18, 19].

The structure that we study, shown in figure 1, consists of a DBH where the two lowest states localized in the well have energies ϵ_0 and ϵ_1. The system is tailored such that when the first excited level is above the left-hand Fermi level ϵ_F^L, $\Delta\epsilon = \epsilon_1 - \epsilon_0$ is slightly smaller than the energy $\hbar\omega_1$ of the LO phonon in the well. The system is under the influence of an external applied potential V. If the Fermi level ϵ_F^L is less than $\Delta\epsilon$, for some value of the gate potential V, the level ϵ_0 drops below the bottom of the conduction band and the current is almost suppressed before the level ϵ_1 falls below the Fermi level. Increasing V, the current flows through the excited level but, as $\Delta\epsilon$ remains less than $\hbar\omega_1$, there is still very little phonon

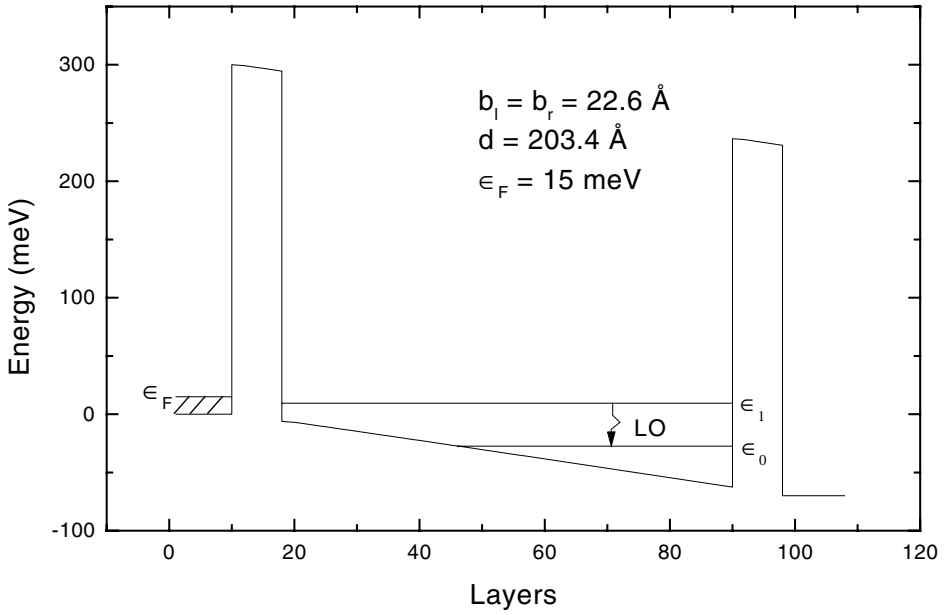

Figure 1. The DBH profile and the electron energy levels close to the resonant condition $\Delta\epsilon \sim \hbar\omega_1$. The width of the barriers (made of $Al_xGa_{1-x}As$) is 22.6 Å and the width of the well (made of GaAs) is 203.4 Å.

emission. After scattering with a phonon, there are no empty states available for the electron to go into which conserve the total energy. However, as $\Delta\epsilon$ increases slightly with V, there is a value of the bias V_0 for which the resonant condition $\Delta\epsilon \sim \hbar\omega_1$ is achieved for the electrons that enter the well. Since electrons remain confined in the well for a long time due to the wide barriers of the heterostructure, they can decay to the ϵ_0-state by emitting a LO phonon. The phonon emission is resonant for these values of the system parameters and it is reasonable to expect a sudden increase of the phonon population.

The LO phonons have a very flat dispersion relation for the wavevector with which they are generated. Therefore they have a very small group velocity. Moreover, for the Al concentration considered in this paper ($x = 0.4$) the LO phonons are also confined inside the well [20, 21] because their frequency is within the range of the phonon gap of the barriers. Due to this, the LO phonons can be also absorbed, exciting electrons from ϵ_0 to ϵ_1. This process proceeds in parallel with the decay of primary phonons due to anharmonicity effects. Their lifetime is short, preventing them from leaving the well. For a GaAs well they decay by anharmonicity into a pair of $\widetilde{\text{LO}}$ and TA phonons in the [111] direction [16, 17].

The TA phonons have a very long lifetime [18] and a mean free path of ∼2 mm [19]. These secondary TA phonons are very interesting because they can constitute an intense coherent beam that is potentially useful for various applications, mainly in acoustic nanoscopy.

Several review articles relate to the device studied here. The generation of pulses of terahertz coherent optical phonons was discussed by Merlin [22]. Coherent phonons can be generated by intense laser pulses [23–27]. A detailed discussion can be found in the review of Kurz *et al* [28]. Stimulated emission of phonons and several kinds of saser were also discussed [30–40]. Among the potential applications of our saser we stress acoustic nanoscopy [41]. At lower frequencies, acoustic microscopy has a wide range of research and industrial applications. Recent reviews can be found in references [42] and [43].

3. The polaronic model

In this section we describe the model used to calculate the electronic current through the DBH including the influence of the electron–phonon interaction.

In our previous calculation [13] we evaluated the electronic current by using the simplest formalism, i.e., sequential tunnelling through a single resonant level (the first excited level) in the well. This is a formalism for resonant tunnelling (because a level in the well appears due to resonance) valid when other levels are far apart from the ground state. The calculation of the incoming current did not take into account the effect of the electron–phonon interaction.

This formalism is clearly not accurate for the case in which the energy of the first excited level in the well is close to the energy of the first satellite of the ground state. This is precisely the resonant condition studied here. The strong electron–phonon (e–ph) interaction prevents these levels from approaching. The states corresponding to these levels are mixed by the e–ph interaction which produces two polaronic levels [3, 4]. This situation will be discussed below in detail.

Our system is described by the Hamiltonian

$$\mathcal{H} = \mathcal{H}_0 + \mathcal{H}_{int} \tag{1}$$

where $\mathcal{H}_0$ is the single-particle Hamiltonian given by an electronic part $\mathcal{H}_e$ plus the contributions $\mathcal{H}_{ph}$ for the phonons:

$$\mathcal{H}_0 = \mathcal{H}_e + \mathcal{H}_{ph}. \tag{2}$$

$\mathcal{H}_{int}$ is the Hamiltonian that describes the electron–phonon and phonon–phonon interactions:

$$\mathcal{H}_{int} = \mathcal{H}_{e-ph} + \mathcal{H}_{ph-ph}. \tag{3}$$

The electron–electron interaction is taken into account by solving self-consistently for the level positions as functions of the accumulated charge. This procedure was discussed in more detail in reference [13].

3.1. The Hamiltonian for electrons

The electronic system is described by a tight-binding Hamiltonian with nearest-neighbour hoppings v. The Hamiltonian can be written in the Wannier basis in terms of the electronic creation and annihilation operators $c^{\dagger}_{lmj\sigma}$, $c_{lmj\sigma}$ at sites lmj with spin σ as

$$\mathcal{H}_e = \sum_{lmj\sigma} \varepsilon_{lmj\sigma} c^{\dagger}_{lmj\sigma} c_{lmj\sigma} + v \sum_{\langle lmj, l'm'j'\rangle\sigma} (c^{\dagger}_{lmj\sigma} c_{l'm'j'\sigma} + c^{\dagger}_{l'm'j'\sigma} c_{lmj\sigma}) \tag{4}$$

where $l, m, j = -\infty, \ldots, \infty$ label the positions for the directions $\boldsymbol{x}$, $\boldsymbol{y}$, $\boldsymbol{z}$, respectively.

The system has no magnetic solutions. Therefore the results are the same for both values of σ and we can drop that subscript. Because the system has translational symmetry in the directions perpendicular to the growth direction ($\boldsymbol{z}$), the Hamiltonian can be uncoupled. We expand the operators c_{lmj} in plane waves in the xy-direction:

$$c_{lmj} = \sum_{\boldsymbol{k}} c_{j\boldsymbol{k}} \mathrm{e}^{\mathrm{i}\boldsymbol{k}\cdot\boldsymbol{x}_{lm}}. \tag{5}$$

By doing that, we can treat the system as a sum over 1D Hamiltonians for each wavevector $\boldsymbol{k}$ perpendicular to the current in the z-direction:

$$\mathcal{H}_e = \sum_{\boldsymbol{k}} \left\{ \sum_{j} \varepsilon_{j\boldsymbol{k}} c^{\dagger}_{j\boldsymbol{k}} c_{j\boldsymbol{k}} + v \sum_{\langle jj'\rangle} (c^{\dagger}_{j\boldsymbol{k}} c_{j'\boldsymbol{k}} + c^{\dagger}_{j'\boldsymbol{k}} c_{j\boldsymbol{k}}) \right\} \tag{6}$$

i.e.,

$$\mathcal{H}_e = \sum_{\boldsymbol{k}} \mathcal{H}_{e\boldsymbol{k}}. \tag{7}$$

The energies $\varepsilon_{j\boldsymbol{k}}$, measured from the bottom of the conduction band of the emitter, are $\varepsilon_{j\boldsymbol{k}} = \varepsilon_j + \varepsilon_{\boldsymbol{k}}$. The energies ε_j are chosen to describe the energy profile of the DBH.

For the sake of simplicity we will leave implicit the dependence on $\boldsymbol{k}$ of the $c_{j\boldsymbol{k}}$-operators. For each $\boldsymbol{k}$ we separate the electronic Hamiltonian $\mathcal{H}_{e\boldsymbol{k}}$ into a part $\mathcal{H}_z$ that depends only on j and another, $\mathcal{H}_\perp$, depending only on $\boldsymbol{k}$:

$$\mathcal{H}_{e\boldsymbol{k}} = \mathcal{H}_\perp + \mathcal{H}_z \tag{8}$$

with

$$\mathcal{H}_z = \sum_j \varepsilon_j c_j^\dagger c_j + v \sum_{\langle jj' \rangle} (c_j^\dagger c_{j'} + c_{j'}^\dagger c_j) \tag{9}$$

and

$$\mathcal{H}_\perp = \varepsilon_{\boldsymbol{k}} \sum_j c_j^\dagger c_j. \tag{10}$$

The last part is, for each $\boldsymbol{k}$, proportional to the identity. Therefore, we can diagonalize the one-dimensional Hamiltonian $\mathcal{H}_z$ independently of $\mathcal{H}_\perp$. We will show first that this one-dimensional Hamiltonian can be reduced to a homogeneous chain with only two different sites necessary to describe the DBH.

For the z-direction we separate the space into three regions: the dispersion region and two semi-infinite homogeneous chains. For $j \leqslant 0$ the planes have energies $\varepsilon_j = -2v$ ($v \leqslant 0$) and for $j \geqslant L+1$ the energies are $\varepsilon_j = -2v - eV$. These values are chosen in order to get the bottom of the conduction band at $\hbar\omega = 0$ for the emitter and at $\hbar\omega = -eV$ for the collector. Here L is the length of the DBH. The corresponding eigenstates of these two regions are plane waves in the z-direction. We disconnect the DBH from the left-hand and right-hand chains. Therefore we get for this region the profile of an infinite (even not rectangular) well, shown in figure 2. For this dispersion region we numerically diagonalize the three-diagonal matrix of order L corresponding to this profile, getting the eigenvalues ε_m and the eigenvectors $|m\rangle$ of the equation

$$\mathcal{H}_z'|m\rangle = \varepsilon_m|m\rangle. \tag{11}$$

Here, $\mathcal{H}_z'$ is the part of $\mathcal{H}_z$ that goes from the beginning of the left-hand barrier to the end of the right-hand one as indicated in figure 2. Written in the basis of planes this is

$$\mathcal{H}_z' = \begin{pmatrix} \varepsilon_1 & v & 0 & \cdots & & 0 \\ v & \varepsilon_2 & v & & & \vdots \\ 0 & v & \varepsilon_3 & \ddots & & \vdots \\ \vdots & & \ddots & \ddots & & \\ \vdots & & & & \varepsilon_{L-1} & v \\ 0 & \cdots & & & v & \varepsilon_L \end{pmatrix}. \tag{12}$$

After the diagonalization we have L levels labelled by $m = 0, \overline{0}, \ldots$.

For the right-hand chain we rename planes $L+1, L+2, \ldots, \infty$ as planes $\underline{1}, \underline{2}, \ldots, \infty$; and for the left-hand one, we rename planes $0, -1, -2, \ldots, -\infty$ as planes $\overline{1}, \overline{2}, \ldots, \overline{\infty}$. Therefore we get a new picture where we have two semi-infinite chains, the first one corresponding to the planes $j = \overline{\infty}, \ldots, \overline{1}$ and the other one corresponding to planes

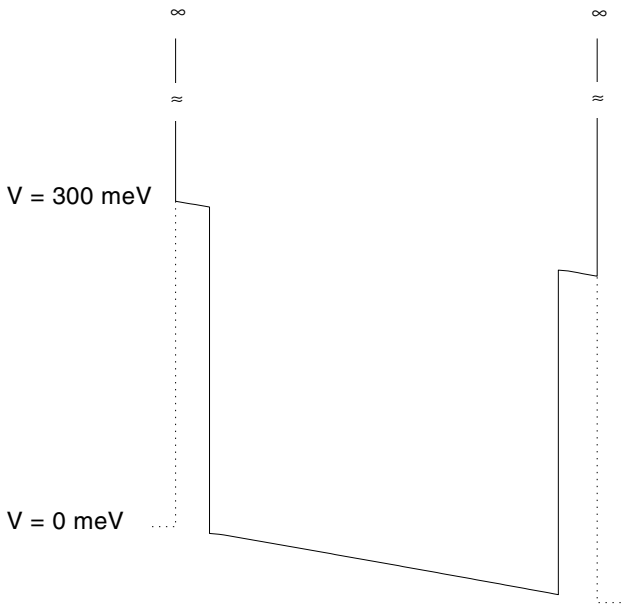

Figure 2. The profile for the scattering region, when we take for the effective hoppings $v_{jm} = 0$. We get a set of discrete levels labelled $0, \bar{0}, \bar{\bar{0}}, \ldots$. Only the two first levels are relevant here.

$j = 1, \ldots, \infty$. Among the L levels obtained from the diagonalization of the matrix (12), only the two states with lower energies will participate significantly in the electronic transport. For the conditions for saser action, discussed here, the other levels are far above the Fermi energy of the emitter. Therefore the dispersion region is represented by $m = 0$ for the ground state and $m = \bar{0}$ for the first excited state with energies ε_0 and $\varepsilon_{\bar{0}}$ respectively (which were called ϵ_0 and ϵ_1 in the introduction).

To connect the DBH with the left-hand and right-hand chains we evaluate the matrix elements

$$v_{jm} = \langle j|\mathcal{H}_z|m\rangle. \tag{13}$$

Only four values are relevant in our calculations: $v_{\bar{1}\bar{0}}$, $v_{\bar{1}0}$, $v_{\bar{0}1}$ and v_{01}. Finally we get for $\mathcal{H}_z$

$$\mathcal{H}_z = \sum_j \varepsilon_j c_j^\dagger c_j + v_{\bar{1}\bar{0}}(c_{\bar{1}}^\dagger c_{\bar{0}} + c_{\bar{0}}^\dagger c_{\bar{1}}) + v_{\bar{1}0}(c_{\bar{1}}^\dagger c_0 + c_0^\dagger c_{\bar{1}}) + v_{\bar{0}1}(c_{\bar{0}}^\dagger c_1 + c_1^\dagger c_{\bar{0}}) + v_{01}(c_0^\dagger c_1 + c_1^\dagger c_0) + \sum_{j\neq\bar{1},0,\bar{0}} v(c_j^\dagger c_{j+1} + c_{j+1}^\dagger c_j). \tag{14}$$

This Hamiltonian is represented diagrammatically in figure 3, in which each point represents an energy ε_j and each line a hopping v.

3.2. The phonon Hamiltonian

As is well known [3,29], the dominant dispersion process for electrons in polar semiconductors is that due to the coupling between electrons and LO phonons. In this work it is essential to consider the $\widetilde{\text{LO}}$ and the TA phonons resulting from the decay of the LO phonons.

The Hamiltonians $\mathcal{H}_{\text{LO}}$, $\mathcal{H}_{\widetilde{\text{LO}}}$, $\mathcal{H}_{\text{TA}}$ used here are the simplest for each kind of phonon considering just one mode in the z-direction. In principle, before the system begins to

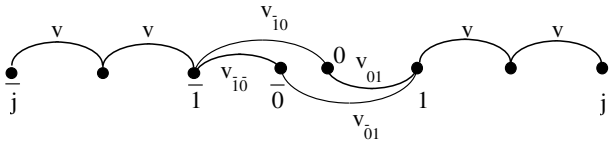

Figure 3. The diagram for the hopping terms in the absence of e–ph interaction. The lines represent the hopping terms. The points represent the plane energies.

exhibit the saser action, several modes, corresponding to several values of the wavevector $\boldsymbol{q}$ perpendicular to the current, are possible for each kind of phonon. However, when the system enters the saser regime the first unstable mode of the TA phonons slaves the others, as also occurs in a laser [44]. This mode is selected by the phonon mirrors (i.e., the walls of the well) and corresponds to $\boldsymbol{q}_3 = 0$ in the direction parallel to the interfaces. Therefore the Hamiltonians required to describe the phonon system are

$$\mathcal{H}_{ph} = \mathcal{H}_{\mathrm{LO}} + \mathcal{H}_{\widetilde{\mathrm{LO}}} + \mathcal{H}_{\mathrm{TA}} \tag{15}$$

with

$$\mathcal{H}_{\mathrm{LO}} = \sum_{\boldsymbol{q}_1} \hbar\omega_1 b^{\dagger}_{1\boldsymbol{q}_1} b_{1\boldsymbol{q}_1} \tag{16}$$

$$\mathcal{H}_{\widetilde{\mathrm{LO}}} = \sum_{\boldsymbol{q}_2} (\hbar\omega_2 - \mathrm{i}\hbar\kappa_2) b^{\dagger}_{2\boldsymbol{q}_2} b_{2\boldsymbol{q}_2} \tag{17}$$

$$\mathcal{H}_{\mathrm{TA}} = (\hbar\omega_3 - \mathrm{i}\hbar\kappa_3) b^{\dagger}_3 b_3 \tag{18}$$

where $\hbar\omega_1, \hbar\omega_2, \hbar\omega_3$ are the energies for LO, $\widetilde{\mathrm{LO}}$ and TA phonons respectively and $b^{\dagger}_j$, b_j are the creation and annihilation operators for phonons. Here we introduced two imaginary terms $\mathrm{i}\hbar\kappa_2$ and $\mathrm{i}\hbar\kappa_3$ that take into account the decay by anharmonicity of the $\widetilde{\mathrm{LO}}$ phonons and the escape of the TA phonons, respectively. The decay of the LO phonons is described in detail by the term $\mathcal{H}_{ph-ph}$. This term is important because it describes the stimulated emission of TA phonons which is the main process in our device.

3.3. The electron–phonon interaction

The electron–phonon interaction is relevant only inside the well. Therefore the e–ph Hamiltonian is written as

$$\mathcal{H}_{e-ph} = \sum_{\boldsymbol{k}\boldsymbol{k}'} g_{\boldsymbol{k}\boldsymbol{k}'} (c^{\dagger}_{0\boldsymbol{k}'} c_{\bar{0}\boldsymbol{k}} b^{\dagger}_{1\boldsymbol{q}} + c^{\dagger}_{\bar{0}\boldsymbol{k}} c_{0\boldsymbol{k}'} b_{1\boldsymbol{q}}) \tag{19}$$

where $g_{\boldsymbol{k}\boldsymbol{k}'}$ is the transition matrix element connecting a state of sub-band $\varepsilon_{\bar{0}\boldsymbol{k}}$ with wavevector parallel to the interface $\boldsymbol{k}$ and the state of the other sub-band $\varepsilon_{0\boldsymbol{k}'}$ with wavevector $\boldsymbol{k}'$. The LO phonon wavevector is $\boldsymbol{q} = \boldsymbol{k}' - \boldsymbol{k}$. The first term in (19) describes the LO phonon emission whereas the second describes the phonon absorption. In order to recover the translational symmetry in the xy-plane we take an average over $\boldsymbol{k}'$ as was done in reference [13]. Therefore we can write the Hamiltonian as

$$\mathcal{H}_{e-ph} = \sum_{\boldsymbol{k}} \mathcal{H}_{e-ph,\boldsymbol{k}} \tag{20}$$

where

$$\mathcal{H}_{e-ph,\boldsymbol{k}} = g(c^{\dagger}_{0\boldsymbol{k}} c_{\bar{0}\boldsymbol{k}} b^{\dagger}_{1\boldsymbol{k}} + c^{\dagger}_{\bar{0}\boldsymbol{k}} c_{\boldsymbol{k}} b_{1\boldsymbol{k}}). \tag{21}$$

We will show in the next section that the electron–phonon interaction mixes the ε_0- and $\varepsilon_{\bar{0}}$-states, producing two polaronic branches.

In a previous work [13] this matrix element was calculated using the simplest electron and phonon states reliable for this system [45–47]. Here we calculate the matrix element $g_{kk'}$ using the more realistic phonon states in the continuum model introduced by Huang and Zhu [48,49] which are similar to those obtained in more sophisticated microscopic calculations [50–52].

The effective coupling g is obtained by averaging over $\boldsymbol{k}$ and $\boldsymbol{k}'$. The averaging procedure is shown in appendix A. It is done in such a way that, from this effective g, one obtains the same LO phonon emission rate w as is calculated from $g_{kk'}$.

The effective g as a function of the applied bias is shown in figure 4. Figure 5 shows the transition rate w calculated from g in comparison with that used in reference [13] using the basis of Licari and Evrard [45, 49]. As was discussed in that previous paper [13] the precise value of w is not relevant to the saser intensity for most of the applied potentials V. Nevertheless, the value of g is important because it determines the separation of the polaronic branches. For this reason the use of the more appropriated basis of Huang and Zhu is important in this work.

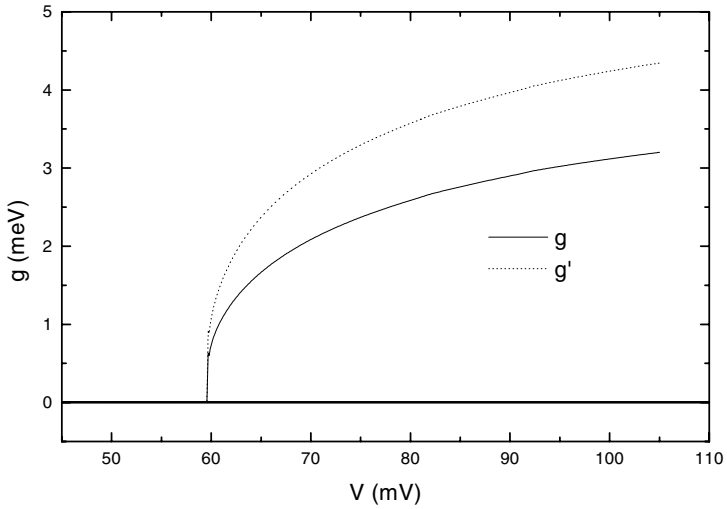

Figure 4. The effective electron–phonon matrix element g as a function of V. The solid line g shows the result obtained using the model of Huang and Zhu. The dotted line g' is the result for the slab model of Licari and Evrard.

3.4. The phonon–phonon interaction

In this paper the phonon–phonon interaction that produces the decay of LO phonons by anharmonicity will be studied using the simplest model treated by Klemens [53]. The phonon–phonon Hamiltonian can be written as

$$\mathcal{H}_{ph-ph} = \gamma(b_1 b_2^\dagger b_3^\dagger + b_1^\dagger b_2 b_3). \tag{22}$$

This Hamiltonian describes the decay LO $\rightarrow \widetilde{\text{LO}}$+TA and its inverse process (recombination). Standard perturbation theory gives for this interaction a decay rate [53] of

$$\frac{\mathrm{d}n_1}{\mathrm{d}t} = \gamma_0[(n_1+1)n_2 n_3 - n_1(n_2+1)(n_3+1)]. \tag{23}$$

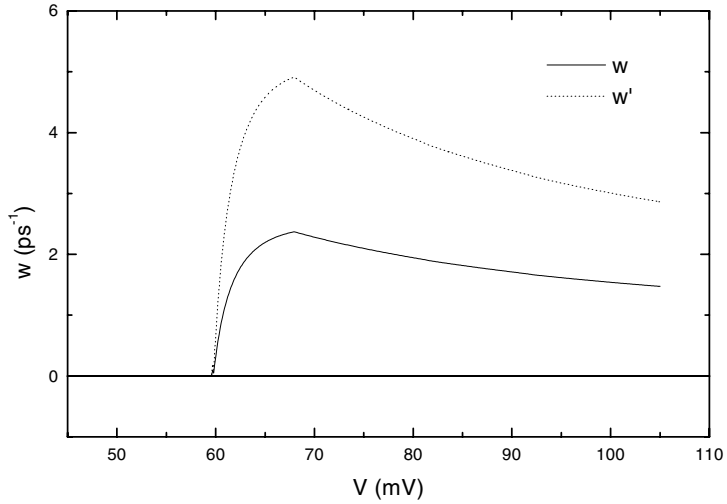

Figure 5. The LO phonon emission rate obtained using the g of Huang and Zhu is shown by the solid line w. The rate obtained from the g' of the slab model is represented by the dotted line w'.

4. The solution of the Hamiltonian

The Hamiltonian used here to calculate the incoming current (which is an important parameter of the kinetic equations that govern the populations of the system) includes an electronic part, the LO phonon term and the effective electron–phonon interaction:

$$\begin{aligned}\mathcal{H} = \sum_j \varepsilon_j c_j^\dagger c_j + \sum_{j\neq\bar{1},0,\bar{0}} v(c_j^\dagger c_{j+1} + c_{j+1}^\dagger c_j) + \hbar\omega_1 b_1^\dagger b_1 + v_{\bar{1}\bar{0}}(c_{\bar{1}}^\dagger c_{\bar{0}} + c_{\bar{0}}^\dagger c_{\bar{1}}) \\ + v_{\bar{1}0}(c_{\bar{1}}^\dagger c_0 + c_0^\dagger c_{\bar{1}}) + v_{\bar{0}1}(c_{\bar{0}}^\dagger c_1 + c_1^\dagger c_{\bar{0}}) + v_{01}(c_0^\dagger c_1 + c_1^\dagger c_0) \\ + g(c_0^\dagger c_{\bar{0}} b_1^\dagger + c_{\bar{0}}^\dagger c_0 b_1).\end{aligned} \tag{24}$$

A new formalism first introduced by Anda *et al* [9] and used later by Bonča and Trugman [54] is applied to solve the system. Let us define the operators [9]

$$\mathcal{O}_j^n = \frac{1}{\sqrt{n!}} c_j b_1^n. \tag{25}$$

Here we use n for the LO phonon number instead of n_1, because there is only one kind of phonon in this section. The operators $\mathcal{O}_j^{\dagger n}$ create an orthonormal basis $|jn\rangle$ of states with an electron in the Wannier orbital localized at site j and n LO phonons inside the well, i.e.,

$$|jn\rangle = \mathcal{O}_j^{\dagger n}|0\rangle. \tag{26}$$

They are the eigenstates of $\mathcal{H}$ when $g = 0$. The equations of motion for these operators are calculated from

$$\mathrm{i}\hbar \frac{\mathrm{d}\mathcal{O}_j^n}{\mathrm{d}t} = [\mathcal{O}_j^n, \mathcal{H}]. \tag{27}$$

For the stationary state we obtain

$$\begin{aligned}
\hbar\omega\mathcal{O}_j^n &= (\varepsilon_j + n\hbar\omega_1)\mathcal{O}_j^n + v(\mathcal{O}_{j+1}^n + \mathcal{O}_{j-1}^n) + gnc_{\bar{0}}^\dagger c_{\bar{0}}\mathcal{O}_j^{n-1} \qquad j \neq \bar{1}, 0, \bar{0}, 1 \\
\hbar\omega\mathcal{O}_{\bar{1}}^n &= (\varepsilon_{\bar{1}} + n\hbar\omega_1)\mathcal{O}_{\bar{1}}^n + v_{\bar{1}\bar{0}}\mathcal{O}_{\bar{0}}^n + v_{\bar{1}0}\mathcal{O}_0^n + v\mathcal{O}_{\bar{2}}^n + gnc_0^\dagger c_{\bar{0}}\mathcal{O}_{\bar{1}}^{n-1} \\
\hbar\omega\mathcal{O}_0^n &= (\varepsilon_0 + n\hbar\omega_1)\mathcal{O}_0^n + v_{\bar{1}0}\mathcal{O}_{\bar{1}}^n + v_{01}\mathcal{O}_1^n + gnc_0^\dagger c_{\bar{0}}\mathcal{O}_0^{n-1} + g\mathcal{O}_{\bar{0}}^n b_1^\dagger \\
\hbar\omega\mathcal{O}_{\bar{0}}^n &= (\varepsilon_{\bar{0}} + n\hbar\omega_1)\mathcal{O}_{\bar{0}}^n + v_{\bar{1}\bar{0}}\mathcal{O}_{\bar{1}}^n + v_{\bar{0}1}\mathcal{O}_1^n + gnc_0^\dagger c_{\bar{0}}\mathcal{O}_{\bar{0}}^{n-1} + g\mathcal{O}_0^{n+1} \\
\hbar\omega\mathcal{O}_1^n &= (\varepsilon_1 + n\hbar\omega_1)\mathcal{O}_1^n + v_{\bar{0}1}\mathcal{O}_{\bar{0}}^n + v_{01}\mathcal{O}_0^n + v\mathcal{O}_2^n + gnc_0^\dagger c_{\bar{0}}\mathcal{O}_1^{n-1}.
\end{aligned} \tag{28}$$

The eigenfunctions of the Hamiltonian can be expanded as

$$|\phi\rangle = \sum_{j,n} a_j^n |jn\rangle. \tag{29}$$

By orthonormality, we get the coefficients of $|\phi\rangle$ as $a_j^n = \langle jn|\phi\rangle$.

In terms of the operators $\mathcal{O}_j^n$,

$$a_j^n = \langle 0|\mathcal{O}_j^n|\phi\rangle. \tag{30}$$

Multiplying equation (28) by $\langle 0|$ on the left and by $|\phi\rangle$ on the right we obtain the eigenvalue equations for these coefficients:

$$\begin{aligned}
\hbar\omega a_j^n &= (\varepsilon_j + n\hbar\omega_1)a_j^n + v(a_{j-1}^n + a_{j+1}^n) \qquad j \neq \bar{1}, 0, \bar{0}, 1 \\
\hbar\omega a_{\bar{1}}^n &= (\varepsilon_{\bar{1}} + n\hbar\omega_1)a_{\bar{1}}^n + va_{\bar{2}}^n + v_{\bar{1}0}a_0^n + v_{\bar{1}\bar{0}}a_{\bar{0}}^n \\
\hbar\omega a_0^n &= (\varepsilon_0 + n\hbar\omega_1)a_0^n + v_{\bar{1}0}a_{\bar{1}}^n + v_{01}a_1^n + \sqrt{n}ga_{\bar{0}}^{n-1} \\
\hbar\omega a_{\bar{0}}^n &= (\varepsilon_{\bar{0}} + n\hbar\omega_1)a_{\bar{0}}^n + v_{\bar{1}\bar{0}}a_{\bar{1}}^n + v_{\bar{0}1}a_1^n + \sqrt{n+1}ga_0^{n+1} \\
\hbar\omega a_1^n &= (\varepsilon_1 + n\hbar\omega_1)a_1^n + v_{\bar{0}1}a_{\bar{0}}^n + v_{01}a_0^n + va_2^n.
\end{aligned} \tag{31}$$

This system is represented diagrammatically in figure 6.

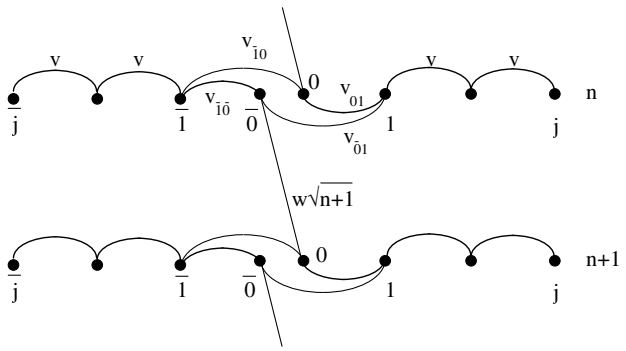

Figure 6. The diagram for the hopping terms in the presence of e–ph interaction. We have a semi-infinite chain in the vertical direction. However, the links to peaks that are above the Fermi level or below the bottom of the conduction band at the emitter can be cut out.

To obtain a strong LO phonon emission it is necessary for the energy difference to reach the resonant condition $\Delta\epsilon \approx \hbar\omega_1$. If the scattering region is isolated, i.e., if the effective hopping terms that connect the well with the external region are put equal to zero, we obtain

$$\hbar\omega a_{\bar{0}}^n = \varepsilon'_{\bar{0}}a_{\bar{0}}^n + \sqrt{n+1}ga_0^{n+1} \tag{32}$$

$$\hbar\omega a_0^{n+1} = \varepsilon'_0 a_0^{n+1} + \sqrt{n+1}ga_{\bar{0}}^n \tag{33}$$

where we have used the notation $\varepsilon'_{\bar{0}} = \varepsilon_{\bar{0}} + n\hbar\omega_1$ and $\varepsilon'_0 = \varepsilon_0 + (n+1)\hbar\omega_1$.

The eigenvalues for these equations are

$$\hbar\omega_{p1,p2} = \frac{\varepsilon'_{\bar{0}} + \varepsilon'_0}{2} \pm \sqrt{\left(\frac{\varepsilon'_{\bar{0}} - \varepsilon'_0}{2}\right)^2 + (n+1)g^2}. \tag{34}$$

The energies $\hbar\omega_{p1}$ and $\hbar\omega_{p2}$ are the energies of the coupled electron–phonon system, i.e., the polaron energies. We can see in figure 7 the behaviour of the electron energies $\varepsilon'_{\bar{0}}$ and ε'_0 and the polaron energies $\hbar\omega_{p1}$ and $\hbar\omega_{p2}$ when the applied potential V is varied. It is clear from equation (34) that when the energy difference $\varepsilon'_{\bar{0}} - \varepsilon'_0$ is much bigger than $\sqrt{n+1}g$, the energy of each polaron branch $\hbar\omega_{pi}$ coincides with either $\varepsilon'_{\bar{0}}$ or ε'_0, whereas if

$$\sqrt{n+1}g \gg \varepsilon'_{\bar{0}} - \varepsilon'_0$$

the separation between branches is $2\sqrt{n+1}g$. As can be seen in figure 4, the effective g increases with the applied potential more rapidly than the difference $\varepsilon'_{\bar{0}} - \varepsilon'_0$. Therefore, the polaronic branches do not approximate the electronic levels before they merge below the bottom of the conduction band. Since the effective hoppings are not zero, these polaronic levels are shifted and broadened.

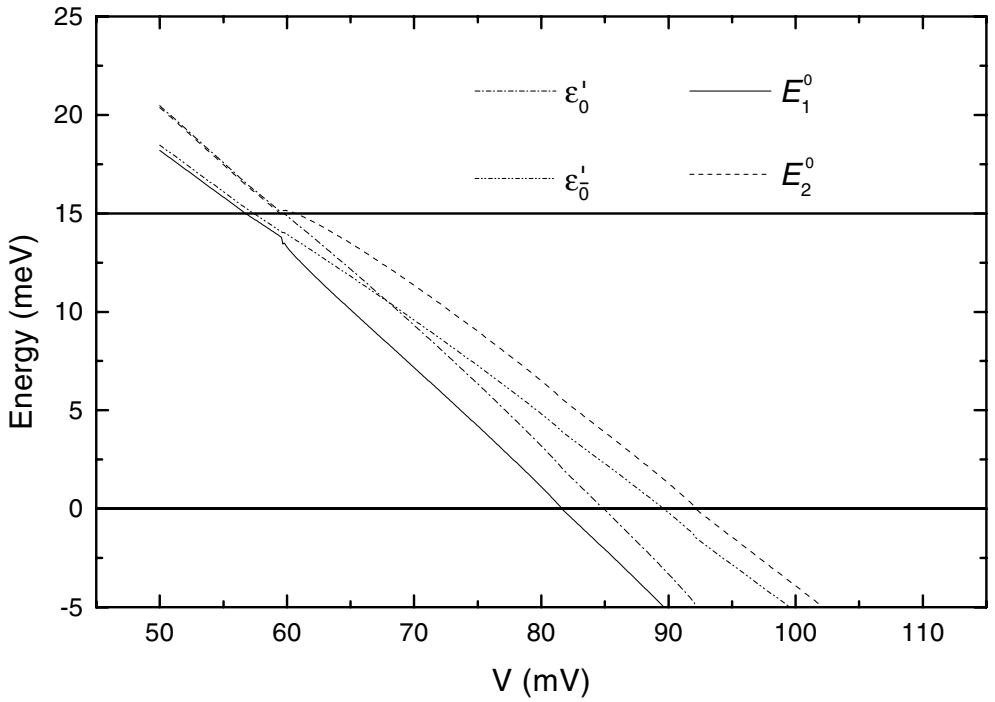

Figure 7. The electronic levels and the polaronic branches as functions of V. $\varepsilon'_{\bar{0}} = \varepsilon_{\bar{0}}$ is the first excited level; $\varepsilon'_0 = \varepsilon_0 + \hbar\omega_1$ is the satellite of the ground state. E_1^0 and E_2^0 are the lower and higher polaronic branches, respectively. The current is very small when E_1^0 is above the Fermi level of the emitter ϵ_F^L or when E_2^0 is below the bottom of the conduction band.

The probability for one electron entering the well to find one LO phonon with momentum $\boldsymbol{q}$ is $p_{\boldsymbol{q}} \sim \langle n_1 \rangle / N_{\boldsymbol{q}}$. Here $\langle n_1 \rangle$ is the average LO phonon number and $N_{\boldsymbol{q}}$ is the number of wavevectors parallel to the interface. We can estimate $N_{\boldsymbol{q}} \sim S_0/a^2$, where S_0 is the device

area and a is the lattice parameter. For the values used here, $S_0 = 0.5 \times 10^{-3}$ mm^2 and $a = 2.825$ Å; N_q is of the order of 7×10^9. The values of $\langle n_1 \rangle$ calculated in this work are less than 35. Therefore $p_q \sim 2 \times 10^{-8}$. That means that we can put $n = 0$ (the subscripts 1 and q were left implicit) in our equations.

The transmittance obtained from the diagram in figure 6 shows peaks that represent, for $g = 0$, the ground state, the first excited state and its satellites. Among these peaks only two are relevant to the current calculation: the first excited state and the satellite of the ground state. The other contributions are at least four orders of magnitude less than those given by the two peaks cited above.

When $g \neq 0$, due to the effect of the electron–phonon interaction, this pair of peaks are mixed in two polaronic branches that anticross.

Since the barriers are broad, the transmittance presents two narrow Lorentzian peaks corresponding to each polaronic branch. These Lorentzian forms are used, in appendix B, to calculate analytical expressions for the input and output currents.

5. Dynamics of electron and phonon populations

In a previous work [13] we derived the kinetic equations that govern the dynamics of electron and phonon populations in the well. The kinetic equations used in this paper are

$$\begin{aligned}
\frac{\mathrm{d}n_{\bar{0}}}{\mathrm{d}t} &= G - w[n_{\bar{0}}(n_1+1) - n_0 n_1] - R_{\bar{0}} n_{\bar{0}} \\
\frac{\mathrm{d}n_0}{\mathrm{d}t} &= w[n_{\bar{0}}(n_1+1) - n_0 n_1] - R_0 n_0 \\
\frac{\mathrm{d}n_1}{\mathrm{d}t} &= w[n_{\bar{0}}(n_1+1) - n_0 n_1] - \gamma_0[n_1(n_2+1)(n_3+1) - (n_1+1)n_2 n_3] \\
\frac{\mathrm{d}n_2}{\mathrm{d}t} &= \gamma_0[n_1(n_2+1)(n_3+1) - (n_1+1)n_2 n_3] - \kappa_2 n_2 \\
\frac{\mathrm{d}n_3}{\mathrm{d}t} &= \gamma_0[n_1(n_2+1)(n_3+1) - (n_1+1)n_2 n_3] - \kappa_3 n_3.
\end{aligned} \tag{35}$$

In spite of the fact that the first two equations are the same as in reference [13], we have used here different parameters. First, the LO phonon emission rate w was calculated from the matrix element g, obtained in section 3.3 using the phonon states proposed by Huang and Zhu [48]. In our previous work the emission rate w was calculated using the simplified model of Licari and Evrard [4]. Besides, the dependence of w upon the applied bias was approximated in reference [13] by a step function with a Gaussian tail. Here we calculated that dependence explicitly; it is shown in figure 5. As we mentioned before, the precise value of w is not relevant to the dynamics when saser action is already developed. Second (and more important), the escape rates $R_{\bar{0}}$ and R_0 used in our previous work were obtained following the work of Jonson [6]. The escape rates in that paper can be interpreted as products of the frequencies of attempts to escape and the probabilities of tunnelling through the right-hand barrier (i.e., the transmittance of that barrier). However, the frequency of attempts was calculated there using the concept of classical velocity. That concept is not applicable for electrons in the lower quantum states in the well. Instead of that, we calculate here $R_m = 2\Gamma_{R_m}/\hbar$ where Γ_{R_m} is the contribution of the right-hand barrier to the width of level m. The expressions obtained here are analogous to those presented by Sols [55]. The values of R_m obtained by this new procedure are, for the same barrier widths, much less than those calculated in [13]. In order to study a system with similar characteristics to those of the previously studied system, we present results for a DBH with thinner barriers. Finally, the input rate G is calculated taking

into account the electron–phonon interaction. In our previous work it was obtained considering only the tunnelling through the excited state in the well. Here we consider also the tunnelling current through the satellite peak and the splitting of the peaks into two polaronic branches. This represents the main modification in the results presented in this work.

In the last three equations we have changed the stimulated LO phonon decay term according to the discussion of section 3.4.

In this paper we restrict ourselves to studying the stationary solutions of the kinetic equations given above:

$$\begin{aligned}
&G - w[n_{\tilde{0}}(n_1+1) - n_0 n_1] - R_{\tilde{0}} n_{\tilde{0}} = 0\\
&w[n_{\tilde{0}}(n_1+1) - n_0 n_1] - R_0 n_0 = 0\\
&w[n_{\tilde{0}}(n_1+1) - n_0 n_1] - \gamma_0[n_1(n_2+1)(n_3+1) - (n_1+1)n_2 n_3] = 0\\
&\gamma_0[n_1(n_2+1)(n_3+1) - (n_1+1)n_2 n_3] - \kappa_2 n_2 = 0\\
&\gamma_0[n_1(n_2+1)(n_3+1) - (n_1+1)n_2 n_3] - \kappa_3 n_3 = 0.
\end{aligned} \tag{36}$$

From these equations, it is easy to obtain all populations in terms of n_3:

$$\begin{aligned}
n_1 &= -\frac{G - \kappa_3 n_3(R_{\tilde{0}}/w + 1)}{G - \kappa_3 n_3(R_{\tilde{0}}/R_0 + 1)}\\
n_2 &= \frac{\kappa_3}{\kappa_2} n_3\\
n_0 &= \frac{\kappa_3}{R_0} n_3\\
n_{\tilde{0}} &= \frac{G - \kappa_3 n_3}{R_{\tilde{0}}}.
\end{aligned} \tag{37}$$

Replacing these expressions in any of the equations (36) containing γ_0, we get a cubic equation for n_3:

$$c_1 c_2 n_3^3 + [(c_2+1)c_3 - c_2 c_4 + c_1 c_5]n_3^2 + [c_3 - (c_2 + c_5 + 1)c_4]n_3 - c_4 = 0 \tag{38}$$

with only one positive root. Here $c_1 = \kappa_3(1/R_{\tilde{0}} + 1/R_0)$, $c_2 = \kappa_3/\kappa_2$, $c_3 = \kappa_3(1/R_{\tilde{0}} + 1/w)$, $c_4 = G/R_{\tilde{0}}$ and $c_5 = \kappa_3/\gamma_0$.

As the input current G, the LO phonon emission rate w and the escape rates R_m depend on the accumulated charge in the well, the electron populations have to be calculated self-consistently. This dependence arises because the level positions depend on the charge. This was discussed in more detail in reference [13].

From these self-consistent solutions we obtain each population as a function of the applied voltage V; these are shown in figures 8 and 9. The saser intensity is the number of TA phonons that escape the well per ps, i.e., $S = \kappa_3 n_3$.

6. Results and conclusions

In this paper we have studied the DBH phonon laser more accurately than previous works [13,14]. The strong electron–phonon interaction near the saser resonance prevents the satellite of the ground state and the first excited level from crossing. We have shown that in this system two polaronic branches appear. As a consequence, the shapes of the $G(V)$ characteristic curve and the saser intensity $S(V)$ are modified.

Moreover, the process of phonon–phonon interaction was considered here in more detail. In our previous works the expression for the LO phonon decay rate was taken from the experimental work of Vallée [17]. As can be seen in the work of Klemens [53], that expression

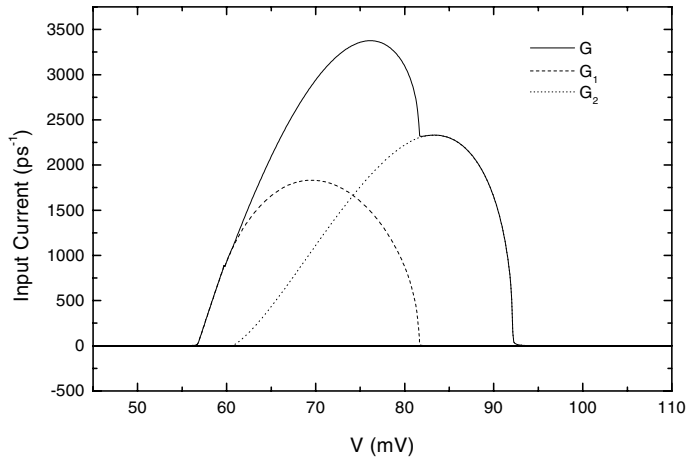

Figure 8. The $G(V)$ characteristic expressed in electrons per ps. We show also the contributions G_i of each polaronic branch.

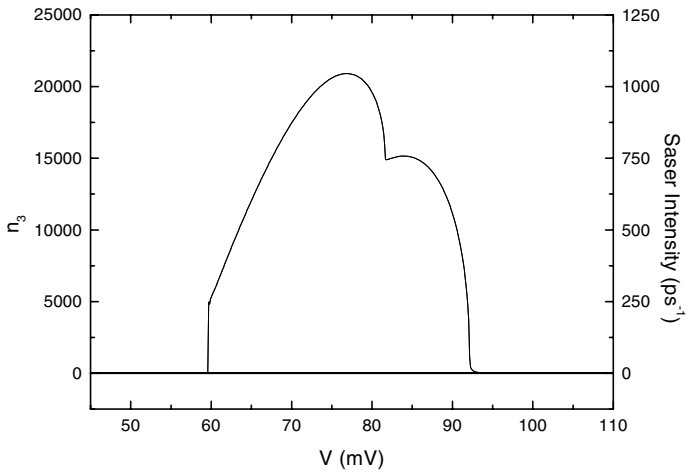

Figure 9. The number n_3 of TA phonons. The saser intensity $S(V) = \kappa_3 n_3$, measured in phonons per ps, is also shown.

is valid only for phonons close to equilibrium. We have used instead the full expression (23) discussed in section 3.4. This causes small changes in the electronic current and the saser intensity but an important variation of the number of LO phonons in the well.

The results are presented for a DBH system composed of an emitter of pure GaAs, a left-hand barrier of width $b_l = 22.6$ Å made of $Al_xGa_{1-x}As$ with an aluminium concentration of $x = 0.4$ that corresponds to a barrier height $V_0 = 300$ meV, a well of width $d = 203.4$ Å of GaAs and a right-hand barrier with the same width and Al concentration as the left-hand barrier. The device area, S_0, was taken equal to 0.5×10^{-3} mm^2. This configuration is shown in figure 1. However, this kind of phonon laser could be built using other structures. For example, in a well made of InP the dimensions of the system could be matched to the LO phonon frequency of this compound. The phonons would then decay coherently by emitting a pair of LA phonons at the middle of the Brillouin zone [17]. However, LA phonons have

short lifetimes. Therefore they are less important for practical applications.

In our tight-binding model we have considered an integer number of planes separated by distances $a = 2.825$ Å. However, the dependence of this lattice parameter on the numerical results is negligible. The hopping v was chosen, as usual, in order to get a dispersion relation at the bottom of the conduction band with the experimental effective mass $m^* = 0.067m_e$, i.e., $v = -\hbar^2/2m^*a^2 = -7150$ meV.

The value of $\gamma_0 = 0.11$ ps^{-1} was taken from the experimental work of Vallée. The escape rate for TA phonons was estimated from the group velocity: $\kappa_3 = 0.05$ ps^{-1}. The decay rate of $\widetilde{\text{LO}}$ phonons was assumed big ($\kappa_2 = 30$ ps^{-1}) because they suffer the stimulation of their decay products. The quantities G, w, $R_{\tilde{0}}$ and R_0 depend on the applied voltage, but typical values are: $G \sim 3000$ ps^{-1}, $w \sim 2$ ps^{-1}, $R_0 \sim 0.025$ ps^{-1} and $R_{\tilde{0}} \sim 0.05$ ps^{-1}.

The characteristic curve $G(V)$ is shown in figure 8. Since we consider a fully resonant tunnelling and since the Fermi energy of the system is smaller than the energy difference between the two lower levels in the well, the current at the valley between the first and second peaks is negligible. In this work we are interested in the region near the saser resonance. Therefore, we show here results for the current around the second peak, which is formed by the superposition of the two polaronic branches. We can see that for small applied bias there is only the contribution of the excited state. The satellite peak only contributes when the peaks corresponding to the ground and the first excited states have a separation sufficiently large to permit transitions between them, via the emission of LO phonons.

The intensity of the phonon beam $S(V)$ follows, after a short instability region, the shape of the current curve. It is easy to show that, when the number of TA phonons n_3 is greater than 10^4, all the terms in equation (38) except the quadratic and cubic ones can be neglected. From that simplified equation we get a linear relation between the saser intensity $S(V) = \kappa_3 n_3$ and the current $G(V)$. This intensity (measured in phonons per ps) is, for the system studied here, of the same order of magnitude as the intensity (in photons per ps) of a commercial laser with a power of about 0.3 mW. The current is directly proportional to the device area. That means that the saser intensity can be easily modified. The linear relation between the amplitude of the phonon beam and the current implies that it could be easily modulated by modulating the input current.

When the electron–phonon interaction begins, the charge in the well increases. This happens because $R_0 < R_{\tilde{0}}$; thus the effective rate of electron escape from the well decreases. This produces an instability in the $G(V)$ characteristics and the saser intensity $S(V)$ at the beginning of the LO phonon emission. The incoming electrons decay to the ground state, then the charge in the well increases sharply. The electron–electron repulsion pushes up the resonant levels in the well and thus they separate, taking the system out of resonance. Therefore the electrons escape directly from the excited level and the charge in the well begins to diminish. When the characteristic times w^{-1} for the LO phonon emission and $R_{\tilde{0}}^{-1}$ for the escape from the excited level are comparable, this produces oscillations that could be chaotic. In the region of instability we cannot obtain self-consistent solutions of equations (36). The iterative process of self-consistency does not converge, which means that the system (35) has no stationary solutions. Similar non-linear effects produce chaotic behaviour in other DBH systems [56–58].

Another consequence of the interrelation between the e–ph interaction and the charge accumulated in the well (the e–e interaction) is the enhancement of the intrinsic bistability [59]. Therefore the hysteresis loop in the current–voltage characteristic becomes more pronounced.

Several effects that were not considered here could restrict the working of the proposed device. The roughness of the barrier walls and the ends of the material could affect the multiple reflections necessary to select just one mode of TA phonons. If the temperature is not low

enough, the noise due to the thermal phonon background could overcome the coherent beam amplitude. The sum of all leak sources has to be smaller than the total gain of the system to warrant the saser action.

The dynamics of the system has to be studied, mainly in the region in which the stationary solutions do not exist. This work is under way and preliminary results were already presented [60]. The model presented here is based on the kinetic equations for the average populations in the well. Quantum fluctuations are not important for large populations, as is the case for electrons and TA phonons. Nevertheless, as the lifetime of LO phonons is very small, their population is small. Therefore these fluctuations are important for them. A full quantum treatment of the system is desirable. This can be done by generalizing the formalism of section 4 to the complete Hamiltonian. This work is being done and the results will be published elsewhere.

Acknowledgments

This work was partially supported by the Brazilian agencies FAPERJ, CNPq and FINEP; and the Latin American agency CLAF.

Appendix. The electron–phonon interaction matrix element

Here we describe the steps used to calculate the matrix element g.

Inside the well, long-wavelength optical phonons can be classified as LO and TO confined modes and interface phonons. The latter have four branches, which, for a symmetric AlGaAs/GaAs/AlGaAs DBH, are the GaAs-like symmetric (S^-) and antisymmetric (A^-) modes, and the corresponding AlGaAs-like modes S^+ and A^+ [62].

The relative strength of the interaction between these modes and electrons depends upon $\boldsymbol{q}d$, where $\boldsymbol{q}$ is the phonon wavevector perpendicular to the current and d is the well width. It can be seen from the energy and momentum conservation relations that, close to the resonance, $\boldsymbol{q}$ is small. For small values of $\boldsymbol{q}d$, the interaction between electrons and interface phonons can be important for DBH with rather thin wells (as, for example, in the case of reference [2], where the satellite phonon peak in the characteristic curve was observed for the first time). Our device has a relatively thick well (about four times the thickness of that of reference [2]). Since the relative importance of the interface phonons decreases strongly when the well width d increases, the effect of these phonons on the electron dynamics should be negligible in our case. This is further confirmed by the results [63] of calculations of the emission rates of confined LO and interface phonons. Moreover, since it is well known (e.g., [64]) that the electron–TO phonon interaction is much weaker than the Fröhlich one, we restrict ourselves to studying the interaction between electrons and just confined LO phonons.

Following the work of Weber and Ryan [49] we consider the general expression for the electron–phonon interaction in the case of LO phonon emission with many possible wavevectors $\boldsymbol{q}$ parallel to the interfaces. The Hamiltonian is

$$\mathcal{H}_{e-ph} = \lambda(S_0 d)^{-1/2} \sum_{n\boldsymbol{q}} \mathrm{e}^{\mathrm{i}\boldsymbol{q}\cdot\boldsymbol{r}} t_n(\boldsymbol{q}) u_n(z)[b_n(\boldsymbol{q}) + b_n^\dagger(-\boldsymbol{q})] \tag{A.1}$$

where $\lambda^2 = 4\pi e^2 \hbar\omega_1(\varepsilon_\infty^{-1} - \varepsilon_0^{-1})$, S_0 is the device area and d is the well width. The parallel component of the displacement $u_n(z)$ is taken from the work of Rudin and Reinecke [61] which modified the Huang and Zhu model [48] for quantum wells:

$$u_n(z) = \begin{cases} \sin(\mu_n \pi z/d) + C_n z/d & \text{for } n = 3, 5, \ldots \\ \cos(\mu_n \pi z/d) - (-1)^{n/2} & \text{for } n = 2, 4, \ldots. \end{cases} \tag{A.2}$$

In this model the first confined mode corresponds to $n = 2$. This is the only mode that we take into account. The integral t_n is given by equation (A1b) of Weber and Ryan:

$$t_2 = (3q^2 + 4\pi^2/d^2)^{-1/2}.$$

Now we calculate the matrix element of $\mathcal{H}_{e-ph}$ connecting states $|\bar{0}, n_1\rangle$ and $|0, n_1 + 1\rangle$. The electron wavefunctions are taken as the simplest for an infinite rectangular well, i.e.,

$$\psi_m = (2/S_0 d)^{-1/2} \sin(m'\pi z/d) \exp(\mathrm{i}\boldsymbol{k}_m \cdot \boldsymbol{r})$$

where $m' = 1, 2$ for $m = 0, \bar{0}$ respectively. The matrix element is

$$g_{\boldsymbol{k}k'} = \langle\bar{0}, n_1|\mathcal{H}_{e-ph}|0, n_1 + 1\rangle = \lambda(S_0 d)^{-1/2} \sum_{\boldsymbol{q}} t_2(\boldsymbol{q})\sqrt{n_1 + 1} \int \mathrm{d}^3 r \; \mathrm{e}^{\mathrm{i}\boldsymbol{q}\cdot\boldsymbol{r}} \psi_{\bar{0}}^* u_2(z) \psi_{\bar{0}}. \tag{A.3}$$

After integration we obtain

$$g_{kk'} = \lambda c(S_0 d)^{-1/2} \sum_{\boldsymbol{q}} t_2(\boldsymbol{q})\sqrt{n_1 + 1}\,\delta_{q-k+k'} \tag{A.4}$$

with $c = 32/(15\pi)$. In order to get an effective g for the simplified Hamiltonian (21) that gives the same LO emission rate, we consider that w, obtained from the Fermi golden rule, is proportional to $\sum_{\boldsymbol{q}} |g_{\boldsymbol{q}}|^2$. Therefore we define

$$g \equiv \sqrt{\sum_{\boldsymbol{q}} |g_{\boldsymbol{q}}|^2} = \sqrt{(S_0/4\pi^2) \int \mathrm{d}\boldsymbol{q} \; |g_{\boldsymbol{q}}|^2}. \tag{A.5}$$

This last integral has to be performed between the same limits as in the calculation of w, i.e., up to a q_{max} given by the conservation of crystalline momentum and energy. The result is

$$g = \frac{\lambda c}{\sqrt{12\pi d}} \left\{ \ln\left[\frac{3}{4} \left(\frac{q_{max}}{q_0} \right)^2 + 1 \right] \right\}^{1/2} \tag{A.6}$$

where

$$q_0 = \frac{\pi}{d} \qquad \text{and} \qquad q_{max}^2 = \frac{2m^*}{\hbar^2} \left[(\varepsilon_F - \varepsilon_{\bar{0}}) + (\varepsilon_F - \varepsilon'_0) + \sqrt{(\varepsilon_F - \varepsilon_{\bar{0}})(\varepsilon_F - \varepsilon'_0)} \right].$$

We can see that for the case where $\varepsilon_{\bar{0}} = \varepsilon'_0$ we get $q_{max} = 2k_{max}$, as expected.

Appendix B. The calculation of the current

In this appendix we describe the way to obtain the analytical expressions for the incoming and the outgoing electronic currents in the saser device. As was done in section 4, we treat here just the LO phonons. We assume here that there are n phonons inside the well.

From the expansion (29) it is immediately apparent that the average number of electrons at site j is

$$\langle n_j \rangle = \sum_n a_j^{n*} a_j^n. \tag{B.1}$$

From the equation of motion for the operators (27) we obtain, for j outside the DBH,

$$\mathrm{i}\hbar \frac{\mathrm{d}a_j^n}{\mathrm{d}t} = (\varepsilon_j + n\hbar\omega_1) a_j^n + v(a_{j-1}^n + a_{j+1}^n). \tag{B.2}$$

Taking the derivative of (B.1) and using (B.2), we obtain the continuity equation

$$\frac{\mathrm{d}\langle n_j \rangle}{\mathrm{d}t} = -(G_j^n - G_{j-1}^n) \tag{B.3}$$

where the contribution of an electron going through channel n to the particle current is

$$G_j^n = \frac{4v}{\hbar}\,\mathrm{Im}(a_{j+1}^{*n} a_j^n). \tag{B.4}$$

The total current is obtained by summing over all channels n and integrating this expression over the Fermi sphere at the emitter:

$$G_j = \frac{4v}{\hbar}\sum_{occ}\sum_{n}\mathrm{Im}(a_{j+1}^{*n} a_j^n). \tag{B.5}$$

It is easy to show that, for the stationary solutions, this expression does not depend on j.

We will obtain now the expression for the current in terms of the reflectance and the transmittances of the double barrier. Outside the DBH, where the profile is flat, the solutions of equations (31) for the coefficients a_j^n are plane waves. On the right we have transmitted waves:

$$a_j^n = A_T^n \mathrm{e}^{\mathrm{i}k'_n z_j} \qquad j \geqslant 1 \tag{B.6}$$

where z_j is the position of plane j, A_T^n is the amplitude of the transmitted wave and the k'_n satisfy the dispersion relation

$$\hbar\omega = n\hbar\omega_1 + 2v[\cos(k'_n a) - 1] - eV.$$

On the left we have two possibilities: if the channel n is above the bottom of the conduction band, the solutions are incident and reflected plane waves:

$$a_j^n = A_I^n \mathrm{e}^{\mathrm{i}k_n z_j} + A_R^n \mathrm{e}^{-\mathrm{i}k_n z_j} \qquad j \leqslant -1. \tag{B.7}$$

Otherwise we have evanescent modes:

$$a_j^n = A_E^n \mathrm{e}^{\kappa_n z_j} \qquad j \leqslant -1. \tag{B.8}$$

Here A_I^n, A_R^n and A_E^n are the amplitudes of the incident wave, the reflected wave and the evanescent mode, respectively. The k_n fulfil the dispersion relation

$$\hbar\omega = n\hbar\omega_1 + 2v[\cos(k_n a) - 1]$$

and the κ_n satisfy

$$\hbar\omega = n\hbar\omega_1 + 2v[\cosh(\kappa_n a) - 1].$$

In terms of the amplitudes for the incident and reflected waves, the expression for the incoming current becomes

$$G = \frac{4v}{\hbar}\sum_{occ}(|A_I^0|^2 - |A_R^0|^2)\sin(k_0 a) \tag{B.9}$$

because the evanescent mode does not contribute to the current. For the outgoing current, the result is

$$G = \frac{4v}{\hbar}\sum_{occ}\sum_{n}|A_T^n|^2 \sin(k'_n a). \tag{B.10}$$

It is easy to prove that, for the stationary states (the only ones that we studied here), the incoming and outgoing currents are the same. The summation over the occupied states can be replaced by an integral over the Fermi sphere at the emitter. The integral over $\boldsymbol{k}$ parallel to the interfaces produces a factor $(k_F^2 - k_z^2)$ that can expressed in terms of $(\epsilon_F^L - \epsilon)$ by approximating the dispersion relation at the bottom of the conduction band by its first (quadratic) term, i.e., $\epsilon = \hbar^2 k_z^2/(2m^*)$. Therefore we can express the incoming current (B.9) as

$$G = \frac{S_0}{2\pi^2}\frac{m^*}{\hbar^3}\int_0^{\epsilon_F^L}\frac{(1-R)}{(1+R+T^0+T^1)}(\epsilon_F^L - \epsilon)\,\mathrm{d}\epsilon \tag{B.11}$$

and the outgoing current is written as

$$G = \frac{S_0}{2\pi^2}\frac{m^*}{\hbar^3}\int_0^{\epsilon_F^L}\frac{[T^0\sin(k_0'a)+T^1\sin(k_1'a)]}{(1+R+T^0+T^1)\sin(k_0a)}(\epsilon_F^L-\epsilon)\,\mathrm{d}\epsilon. \tag{B.12}$$

The denominator $1+R+T^0+T^1$ comes from the normalization of the wavefunction. The factor $\sin(k_0a)$ in the incoming current cancels with the unidimensional density of states at the emitter: $\rho(\epsilon)=[-2va\sin(k_0a)]^{-1}$. In the expressions above, R is the reflectance and T^0 and T^1 the transmittances through the channels without phonons and with one phonon, respectively. They are defined as usual: $R=|r|^2$, $T^0=|t^0|^2$, $T^1=|t^1|^2$, where $r\equiv A_R^0/A_I^0$, $t^0\equiv A_T^0/A_I^0$, $t^1\equiv A_T^1/A_I^0$ are the Fresnel reflection and transmission coefficients. We define also a Fresnel coefficient for the evanescent mode: $r_E\equiv A_E^0/A_I^0$. There is no current on the left through channel 0, as expected, because $a_{j+1}^{*0}a_j^0$ is real for $j\leqslant -1$. Therefore the coefficient r_E is not relevant to the current.

To solve the equations (31) we have to connect the expressions given above for the coefficients a_j^n on the left and on the right of the DBH. To do so, we will make some approximations to uncouple the system.

The solution of the diagram of figure 6 has peaks for the ground state, the first excited state and all its satellites. The peaks relevant to the transport are those related to the first excited level (the channel with n phonons that passes through $\bar{0}$) and the satellite of the ground state (the channel with $n+1$ phonons through 0). The channel with n phonons that passes through 0 gives the contribution of the ground state which is far below the bottom of the conduction band at the emitter. This contribution is completely negligible. The same happens for the channel corresponding to the satellite of the excited state (that passes through $\bar{0}$ with $n+1$ phonons), which is far above the Fermi level. Therefore it is sufficient to solve the simplified diagram of figure B1.

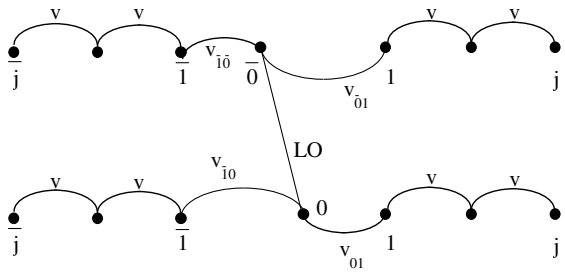

Figure B1. A simplified version of the diagram of figure 6. The links with the second and higher satellites and the hoppings that produce the peak corresponding to the ground state and the first satellite of the first excited state were cut out.

We will show the procedure for the case in which the number of LO phonons in the well is very small. This was suggested by the results of our previous work and confirmed by the present results. We can consider that for each $\boldsymbol{k}$ the average LO phonon number is zero. The system to solve is, for $n=0$,

$$\hbar\omega a_j^0 = \varepsilon_j a_j^0 + v(a_{j-1}^0 + a_{j+1}^0) \qquad j\neq\bar{1},0,\bar{0},1 \tag{B.13}$$

$$\hbar\omega a_{\bar{1}}^0 = va_2^0 + \varepsilon_{\bar{1}}a_{\bar{1}}^0 + v_{\bar{1}\bar{0}}a_{\bar{0}}^0 \tag{B.14}$$

$$\hbar\omega a_{\bar{0}}^0 = v_{\bar{1}\bar{0}}a_{\bar{1}}^0 + \varepsilon_{\bar{0}}a_{\bar{0}}^0 + ga_0^1 + v_{\bar{0}1}a_1^0 \tag{B.15}$$

$$\hbar\omega a_1^0 = v_{\bar{0}1}a_{\bar{0}}^0 + \varepsilon_1 a_1^0 + va_2^0. \tag{B.16}$$

This system is coupled with that for $n = 1$:

$$\hbar\omega a_j^1 = (\varepsilon_j + \hbar\omega_1)a_j^1 + v(a_{j-1}^1 + a_{j+1}^1) \qquad j \neq \bar{1}, 0, \bar{0}, 1 \tag{B.17}$$

$$\hbar\omega a_{\bar{1}}^1 = (\varepsilon_{\bar{1}} + \hbar\omega_1)a_{\bar{1}}^1 + va_{\bar{2}}^1 + v_{\bar{1}0}a_0^1 \tag{B.18}$$

$$\hbar\omega a_0^1 = v_{\bar{1}0}a_{\bar{1}}^1 + ga_{\bar{0}}^0 + (\varepsilon_0 + \hbar\omega_1)a_0^1 + v_{01}a_1^1 \tag{B.19}$$

$$\hbar\omega a_1^1 = v_{01}a_0^1 + (\varepsilon_1 + \hbar\omega_1)a_1^1 + va_2^1. \tag{B.20}$$

We are interested in obtaining the relation between the amplitudes A_I^n, A_R^n, A_T^n and A_E^n. From equations (B.16) and (B.20) we get

$$a_{\bar{0}}^0 = A_T^0 \frac{v}{v_{\bar{0}1}} \tag{B.21}$$

$$a_0^1 = A_T^1 \frac{v}{v_{01}}. \tag{B.22}$$

From (B.14) and (B.18) we get

$$a_{\bar{2}}^0 = 2\cos(k_0 a)a_{\bar{1}}^0 - \frac{v_{\bar{1}\bar{0}}}{v_{\bar{0}1}}A_T^0 \tag{B.23}$$

$$a_{\bar{2}}^1 = 2\cosh(\kappa_1 a)a_{\bar{1}}^1 - \frac{v_{\bar{1}0}}{v_{01}}A_T^1. \tag{B.24}$$

Using the results (B.21), (B.22), (B.23) and (B.24) we get the system

$$\begin{aligned} a_{\bar{1}}^0 &= \alpha A_T^0 + \beta A_T^1 \\ a_{\bar{1}}^1 &= \gamma A_T^0 + \xi A_T^1 \\ a_{\bar{2}}^0 &= 2\cos(k_0 a)a_{\bar{1}}^0 - \frac{v_{\bar{1}\bar{0}}}{v_{\bar{0}1}}A_T^0 \\ a_{\bar{2}}^1 &= 2\cosh(\kappa_1 a)a_{\bar{1}}^1 - \frac{v_{\bar{1}0}}{v_{01}}A_T^1 \end{aligned} \tag{B.25}$$

where

$$\begin{aligned} \alpha &\equiv \frac{[(-\varepsilon_{\bar{0}} + \hbar\omega)v/v_{\bar{0}1} - v_{\bar{0}1}\mathrm{e}^{\mathrm{i}k_0' a}]}{v_{\bar{1}\bar{0}}} \\ \beta &\equiv -\frac{g}{v_{\bar{1}\bar{0}}}\frac{v}{v_{01}} \\ \gamma &\equiv -\frac{g}{v_{\bar{1}0}}\frac{v}{v_{\bar{0}1}} \\ \xi &\equiv \frac{[(-\varepsilon_0 - \hbar\omega_1 + \hbar\omega)v/v_{01} - v_{01}\mathrm{e}^{\mathrm{i}k_1' a}]}{v_{\bar{1}0}}. \end{aligned} \tag{B.26}$$

From the relations (B.7) and (B.8) we get for $a_{\bar{1}}^0$, $a_{\bar{1}}^1$, $a_{\bar{2}}^0$ and $a_{\bar{2}}^1$

$$\begin{aligned} a_{\bar{1}}^0 &= A_I^0\mathrm{e}^{-\mathrm{i}k_0 a} + A_R^0\mathrm{e}^{\mathrm{i}k_0 a} \\ a_{\bar{1}}^1 &= A_E\mathrm{e}^{-\kappa_0 a} \\ a_{\bar{2}}^0 &= A_I^0\mathrm{e}^{-2\mathrm{i}k_0 a} + A_R^0\mathrm{e}^{2\mathrm{i}k_0 a} \\ a_{\bar{2}}^1 &= A_E\mathrm{e}^{-2\kappa_1 a}. \end{aligned} \tag{B.27}$$

Using (B.27) and (B.25) we get

$$\begin{aligned}
&\alpha t^0 + \beta t^1 - r\mathrm{e}^{\mathrm{i}k_0 a} = \mathrm{e}^{-\mathrm{i}k_0 a} \\
&\left(2\alpha\cos(k_0 a) - \frac{v_{\bar{1}\bar{0}}}{v_{\bar{0}1}}\right)t^0 + 2\beta\cos(k_0 a)t^1 - r\mathrm{e}^{2\mathrm{i}k_0 a} = \mathrm{e}^{-2\mathrm{i}k_0 a} \\
&\gamma t^0 + \xi t^1 - r_E\mathrm{e}^{-\kappa_1 a} = 0 \\
&-\frac{v_{\bar{1}0}}{v_{01}}t^1 + r_E = 0.
\end{aligned} \tag{B.28}$$

To write the solutions of the system (B.28) in a compact form we define the complex energies

$$\widetilde{\varepsilon}_0 \equiv \varepsilon_0' + \Delta_0 - \mathrm{i}\Gamma_0 \tag{B.29}$$

$$\widetilde{\varepsilon}_{\bar{0}} \equiv \varepsilon_{\bar{0}} + \Delta_{\bar{0}} - \mathrm{i}\Gamma_{\bar{0}} \tag{B.30}$$

where $\Delta_{\bar{0}}$, Δ_0, $\Gamma_{\bar{0}}$ and Γ_0 are defined as

$$\Delta_{\bar{0}} \equiv \frac{v_{\bar{0}1}^2}{v}\cos(k_0' a) + \frac{v_{\bar{1}\bar{0}}^2}{v}\cos(k_0 a) \tag{B.31}$$

$$\Delta_0 \equiv \frac{v_{01}^2}{v}\cos(k_1' a) + \frac{v_{\bar{1}0}^2}{v}\mathrm{e}^{-(\kappa_1 a)} \tag{B.32}$$

$$\Gamma_{\bar{0}} \equiv -\frac{v_{\bar{0}1}^2}{v}\sin(k_0' a) - \frac{v_{\bar{1}\bar{0}}^2}{v}\sin(k_0 a) \tag{B.33}$$

$$\Gamma_0 \equiv -\frac{v_{01}^2}{v}\sin(k_1' a). \tag{B.34}$$

In terms of these complex energies the Fresnel coefficients are written as

$$t^0 = \mathcal{A}(\hbar\omega)v_{\bar{0}1}(\hbar\omega - \widetilde{\varepsilon}_0) \tag{B.35}$$

$$t^1 = \mathcal{A}(\hbar\omega)g v_{01} \tag{B.36}$$

$$r = -1 + \mathcal{A}(\hbar\omega)v_{\bar{0}\bar{1}}(\hbar\omega - \widetilde{\varepsilon}_0) \tag{B.37}$$

$$r_E = \mathcal{A}(\hbar\omega)g v_{\bar{1}0}. \tag{B.38}$$

where

$$\mathcal{A}(\hbar\omega) = \frac{-2\mathrm{i}\sin(k_0 a)v_{\bar{1}\bar{0}}/v}{(\hbar\omega - \widetilde{\varepsilon}_{\bar{0}})(\hbar\omega - \widetilde{\varepsilon}_0) - g^2}. \tag{B.39}$$

If we put $g = 0$ in equations (B.35), (B.36) and (B.37), we get, for the current, two Lorentzian peaks at energies $\varepsilon_m + \Delta_m$ of width Γ_m. This result is consistent with those of Wingreen *et al* [5] and Sols [55] obtained using the Green function formalism for uncoupled resonant peaks.

If we disconnect the well (taking $v_{jm} = 0$) but keep the electron–phonon interaction ($g \neq 0$), we recover the eigenvalue system (33) whose solutions are given by (34).

The denominator of expressions (B.35), (B.36) and (B.37) is quadratic in $\hbar\omega$. It has two complex roots that are the poles of the Fresnel coefficients t^1, t^0 and r:

$$E_{2,1} = \frac{(\widetilde{\varepsilon}_{\bar{0}} + \widetilde{\varepsilon}_0)}{2} \pm \frac{1}{2}\sqrt{(\widetilde{\varepsilon}_0 - \widetilde{\varepsilon}_{\bar{0}})^2 + 4g^2} \qquad \mathrm{Re}(E_2) > \mathrm{Re}(E_1). \tag{B.40}$$

In terms of these complex eigenvalues we can write

$$\mathcal{A}(\hbar\omega) = \frac{-2\mathrm{i}\sin(k_0 a)v_{\bar{1}\bar{0}}/v}{(\hbar\omega - E_1)(\hbar\omega - E_2)}. \tag{B.41}$$

We can easily estimate the positions E_i^0 and the widths Γ_i of each of the polaronic peaks, which are given by the real and imaginary parts of E_i, respectively (equation (B.40)), as

$$E_i = E_i^0 - \mathrm{i}\Gamma_i \qquad i = 1, 2. \tag{B.42}$$

By defining the variations $\delta\varepsilon = \varepsilon'_0 - \varepsilon_{\bar{0}}$, $\delta\Delta = \Delta_0 - \Delta_{\bar{0}}$ and $\delta\Gamma = \Gamma_0 - \Gamma_{\bar{0}}$, we can write $\widetilde{\varepsilon}_0 - \widetilde{\varepsilon}_{\bar{0}} = \delta\varepsilon + \delta\Delta - \mathrm{i}\,\delta\Gamma$. As the product $(\delta\varepsilon + \delta\Delta)\delta\Gamma$ is very small, we can approximate the square root in (B.40) by

$$\frac{1}{2}\sqrt{(\widetilde{\varepsilon}_0 - \widetilde{\varepsilon}_{\bar{0}})^2 + 4g^2} \cong \frac{1}{2}\left[(\delta\varepsilon + \delta\Delta)^2 + 4g^2\right]^{1/2} + \frac{\mathrm{i}}{2}\frac{(\delta\varepsilon + \delta\Delta)\delta\Gamma}{\left[(\delta\varepsilon + \delta\Delta)^2 + 4g^2\right]^{1/2}}. \tag{B.43}$$

Now, if we define

$$E_M = \frac{1}{2}\left[(\varepsilon_{\bar{0}} + \Delta_{\bar{0}}) + (\varepsilon'_0 + \Delta^1)\right] \tag{B.44}$$

$$\Delta_M = \left[(\delta\varepsilon + \delta\Delta)^2 + 4g^2\right]^{1/2} \tag{B.45}$$

$$\Gamma_M = \frac{1}{2}(\Gamma_0 + \Gamma_{\bar{0}}) \tag{B.46}$$

$$\Delta\Gamma_M = \frac{(\delta\varepsilon + \delta\Delta)\delta\Gamma}{\left[(\delta\varepsilon + \delta\Delta)^2 + 4g^2\right]^{1/2}} \tag{B.47}$$

we can write

$$E^0_{2,1} = E_M \pm \frac{1}{2}\Delta_M \tag{B.48}$$

$$\Gamma_{2,1} = \Gamma_M \mp \frac{1}{2}\Delta\Gamma_M. \tag{B.49}$$

Therefore the peaks are localized below and above E_M, separated by Δ_M, and the widths of the peaks are approximately the same, because $\Delta\Gamma$ is very small. In practice we calculate E_i directly from the definition (B.40).

Let us write the expression to be integrated in (B.11) or (B.12) as

$$\mathcal{F}(\hbar\omega)\mathcal{L}_1(\hbar\omega)\mathcal{L}_2(\hbar\omega) \tag{B.50}$$

where the Lorentzians

$$\mathcal{L}_i(\hbar\omega) = \frac{\Gamma_i}{[(\hbar\omega - E^0_i)^2 + \Gamma_i^2]} \tag{B.51}$$

are very narrow. As the peak labelled 1 is always below the peak 2, we can separate the integrals into one over the interval $[0, E_M]$ and another over the interval $[E_M, \varepsilon^L_F]$:

$$\int_0^{\varepsilon^L_F} \mathcal{F}(\hbar\omega)\mathcal{L}_1(\hbar\omega)\mathcal{L}_2(\hbar\omega)\,\mathrm{d}(\hbar\omega) \approx \mathcal{F}(E^0_1)\mathcal{L}_2(E^0_1)\int_0^{E_M}\mathcal{L}_1(\hbar\omega)\,\mathrm{d}(\hbar\omega) + \mathcal{F}(E^0_2)\mathcal{L}_1(E^0_2)\int_{E_M}^{\varepsilon^L_F}\mathcal{L}_2(\hbar\omega)\,\mathrm{d}(\hbar\omega). \tag{B.52}$$

In these expressions we have exploited the fact that in the very small region in which one Lorentzian is not negligible the other factors are essentially constant. The integrals in (B.52) are elementary:

$$\int_0^{\varepsilon^L_F} \mathcal{F}(\hbar\omega)\mathcal{L}_1(\hbar\omega)\mathcal{L}_2(\hbar\omega)\,\mathrm{d}(\hbar\omega) \approx \mathcal{F}(E^0_1)\mathcal{L}_2(E^0_1)[\mathcal{I}_1(E_M) - \mathcal{I}_1(0)] + \mathcal{F}(E^0_2)\mathcal{L}_1(E^0_2)[\mathcal{I}_2(\varepsilon^L_F) - \mathcal{I}_2(E_M)] \tag{B.53}$$

with

$$\mathcal{I}_i(\hbar\omega) = \arctan\left(\frac{\hbar\omega - E^0_i}{\Gamma_i}\right). \tag{B.54}$$

We have performed also the exact (numerical) integrations for the current. The difference is negligible. From the expressions (B.34) and (B.33) we separate out the contribution of the escape through the right-hand barrier. For Γ_0 this is the only contribution because there is no current below the bottom of the conduction band. In the case of $\Gamma_{\bar{0}}$, that contribution is given by the first term of the right-hand side of (B.33). As was discussed in section 5, we get

$$\begin{aligned} R_{\bar{0}} &= -\frac{2v_{\bar{0}1}^2}{\hbar v}\sin(k_0' a) \\ R_0 &= -\frac{2v_{01}^2}{\hbar v}\sin(k_1' a). \end{aligned} \tag{B.55}$$

For a given barrier width, the escape rates given by (B.55) are appreciably smaller than those obtained following the work of Jonson [6].

References

[1] Capasso F and Datta S 1990 *Phys. Today* **43** (2) 74
[2] Goldman V J, Tsui D C and Cunningham J E 1987 *Phys. Rev. Lett.* **58** 1256
Goldman V J, Tsui D C and Cunningham J E 1987 *Phys. Rev.* B **36** 7635
[3] Fröhlich H 1954 *Adv. Phys.* **3** 325
[4] Evrard R 1972 *Polarons in Ionic Crystals and Polar Semiconductors* ed J T Devreese (Amsterdam: North-Holland) pp 29–80
[5] Wingreen N S, Jacobsen V W and Wilkins J W 1989 *Phys. Rev.* B **40** 11 834
[6] Jonson M 1989 *Phys. Rev.* B **39** 5924
[7] Büttiker M 1986 *Phys. Rev. Lett.* **57** 1761
Pastawski H M 1991 *Phys. Rev.* B **44** 6329
[8] Støvneng J A, Hauge E H, Lipavský P and Špička V 1991 *Phys. Rev.* B **44** 13 595
[9] Anda E V, Makler S S, Pastawski H M and Barrera R G 1994 *Braz. J. Phys.* **24** 330
Orellana P, Claro F, Anda E and Makler S 1996 *Phys. Rev.* B **53** 12 967
[10] Anda E V and Flores F 1991 *J. Phys.: Condens. Matter* **3** 9087
Pastawski H M 1992 *Phys. Rev.* B **46** 4053
[11] Lake R, Klimeck G and Datta S 1993 *Phys. Rev.* B **47** 6427
Lake R, Klimeck G, Anantram M P and Datta S 1993 *Phys. Rev.* B **48** 15 132
[12] Zou N and Chao K A 1992 *Phys. Rev. Lett.* **69** 3224
Zou N, Rammer J and Chao K A 1992 *Phys. Rev.* B **46** 15 912
Zou N, Chao K A and Galperin Y M 1993 *Phys. Rev. Lett.* **71** 1756
[13] Makler S S, Vasilevskiy M I, Weberszpil J, Anda E V, Tuyarot D E and Pastawski H M 1998 *J. Phys.: Condens. Matter* **10** 5905
[14] Makler S S, Tuyarot D E, Anda E V and Vasilevskiy M I 1996 *Surf. Sci.* **361+362** 239
[15] Tuyarot D E, Makler S S, Anda E V and Vasilevskiy M I 1996 *Superlatt. Microstruct.* **20** 7279
[16] Vallée F and Bogani F 1991 *Phys. Rev.* B **43** 12 049
[17] Vallée F 1994 *Phys. Rev.* B **49** 2460
[18] Ulbrich R G 1984 *Nonequilibrium Phonon Dynamics (NATO ASI Series vol 124)* ed W E Bron (New York: Plenum) p 114
[19] Ulbrich R G, Narayanamurty V and Chin M A 1980 *Phys. Rev. Lett.* **45** 1432
[20] Jusserand B, Mallot F, Moison J-M and Le Roux G 1990 *Appl. Phys. Lett.* **57** 560
[21] Jacob J M, Kim D M, Bouchalkha A, Sony J J, Klem J F, Hou H, Tu C W and Morkoç H 1994 *Solid State Commun.* **91** 721
[22] Merlin R 1997 *Solid State Commun.* **102** 207
[23] Cho G C, Kutt W and Kurz H 1990 *Phys. Rev. Lett.* **65** 764
[24] Cheng T K, Vidal J, Zeiger H J, Dresselhaus G, Dresselhaus M S and Ippen E P 1991 *Appl. Phys. Lett.* **59** 1923
[25] Pfeifer T, Kutt W, Kurz H and Scholz R 1992 *Phys. Rev. Lett.* **69** 3248
[26] Kutt W, Cho G C, Pfeifer T and Kurz H 1992 *Semicond. Sci. Technol.* **7** B77
[27] Albrecht W, Kruse Th and Kurz H 1992 *Phys. Rev. Lett.* **69** 1452
[28] Kurz H A, Albrecht W and Kurz H 1992 *IEEE J. Quantum Electron.* **28** 2434
[29] Haken H 1976 *Quantum Field Theory of Solids, an Introduction* (Amsterdam: North-Holland) p 218
[30] Bron W E and Grill W 1978 *Phys. Rev. Lett.* **40** 1459

[31] Prieur J-Y, Höhler R, Joffrin J and Devaud M 1993 *Europhys. Lett.* **24** 409
[32] Prieur J-Y, Devaud M, Joffrin J, Barre C, Stenger M and Chevallier M 1996 *Physica* B **219+220** 235
[33] Zavtrak S T 1995 *Phys. Rev.* E **51** 2480
[34] Zavtrak S T 1995 *Phys. Rev.* E **51** 3767
[35] Zavtrak S T 1995 *Zh. Tekh. Fiz.* **65** 123 (Engl. Transl. 1995 *Tech. Phys.* **40** 589)
[36] Zavtrak S T 1996 *J. Acoust. Soc. Am.* **99** 730
[37] Doinikov A A and Zavtrak S T 1996 *J. Acoust. Soc. Am.* **99** 3849
[38] Zavtrak S T and Volkov I V 1997 *Zh. Tekh. Fiz.* **67** 92 (Engl. Transl. 1997 *Tech. Phys.* **42** 406)
[39] Fokker P A, Dijkhuis J I and de Wijn H W 1997 *Phys. Rev.* B **55** 2925
[40] Fokker P A, Melzer R S, Wang Y P, Dijkhuis J I and de Wijn H W 1997 *Phys. Rev.* B **55** 2934
[41] Maris H 1998 *Sci. Am.* **8** (1) 104
[42] Yu Z and Boseck S 1995 *Rev. Mod. Phys.* **67** 863
[43] Gilmore R S 1996 *J. Phys. D: Appl. Phys.* **29** 1389
[44] Haken H 1995 *Rev. Mod. Phys.* **47** 67
Haken H 1978 *Synergetics: an Introduction* (New York: Spinger)
[45] Licari J J and Evrard R 1977 *Phys. Rev.* B **15** 2254
[46] Trallero-Giner C and Comas F 1988 *Phys. Rev.* B **37** 4583
[47] Trallero-Giner C and Comas F 1994 *Phil. Mag.* B **70** 583
[48] Huang K and Zhu B 1989 *Phys. Rev.* B **38** 13 777
[49] Weber G and Ryan J F 1992 *Phys. Rev.* B **45** 11 202
[50] Rücker H, Molinari E and Lugli P 1991 *Phys. Rev.* B **44** 3463
[51] Lugli P, Molinari E and Rücker H 1991 *Superlatt. Microstruct.* **10** 471
[52] Rücker H, Molinari E and Lugli P 1992 *Phys. Rev.* B **45** 6747
[53] Klemens P G 1966 *Phys. Rev.* **148** 845
[54] Bonča J and Trugman S A 1995 *Phys. Rev. Lett.* **75** 2556
Bonča J and Trugman S A 1997 *Phys. Rev. Lett.* **79** 4874
[55] Sols F 1992 *Ann. Phys., NY* **214** 386
[56] Prescilla C, Jona-Lasinio G and Capasso F 1991 *Phys. Rev.* B **43** 5200
[57] Jona-Lasinio G, Prescilla C and Capasso F 1992 *Phys. Rev. Lett.* **68** 2269
[58] Orellana P, Anda E and Claro F 1997 *Phys. Rev. Lett.* **79** 2269
[59] Leadbeater M L, Alves E S, Eaves L, Henini M, Hughes O H, Sheard F W and Toombs G A 1988 *Semicond. Sci. Technol.* **3** 1060
Sheard F W and Toombs G A 1992 *Appl. Phys. Lett.* **52** 1228
[60] Weberszpil J, Makler S S, Anda E V and Vasilevskiy M I 1996 *Proc. ICPS-XXIII: 23rd Int. Conf. on the Physics of Semiconductors (Berlin)* vol 4, p 3299
Weberszpil J, Makler S S, Anda E V and Vasilevskiy M I 1998 *Microelectron. Eng.* **43+44** 471
[61] Rudin S and Reinecke T L 1991 *Phys. Rev.* B **41** 9298
[62] Wendler L and Pechstedt R 1987 *Phys. Status Solidi* b **141** 129
[63] Wendler L, Haupt R, Bechstedt F, Rücker H and Enderline R 1988 *Superlatt. Microstruct.* **4** 577
[64] Wendler L and Haupt R 1991 *Phys. Rev.* B **44** 1850